Mining, Metallurgy & Exploration (2023) 40:563–581
https://doi.org/10.1007/s42461-023-00737-x

# Dynamic Response Analysis of a Reinforced Concrete Structure in Underground Coal Mine Environment with Various Strata Conditions

**Kutay E. Karadeniz[1] · Samuel Nowak[1] · Dogukan Guner[1] · Taghi Sherizadeh[1]**

Received: 4 August 2022 / Accepted: 26 January 2023 / Published online: 8 February 2023


**Abstract**
Seals and build-in-place (BIP) refuge alternatives (RAs) are two main underground structures to isolate an area from the active working zones with different purposes. While seals are used to prevent methane gas that seeps from coal seams and blast pressures from a possible detonation of the contained gas, RAs are used to provide a safe haven for miners who are unable to escape their working locations after an accident like an explosion or fire. The recommended BIP RA designs can be similar to seals constructed with steel-reinforced concrete. Both seal and BIP RA are constructed in different locations of the mines for a period of time, exposed to a certain convergence due to stress redistribution which can change their responses during an explosion. In this study, a steel-reinforced concrete wall to be used in such applications is simulated to examine the structural performance during an explosion for a coal mine model with different strata conditions using dynamic analysis by a 3D distinct element method (DEM) code. The main purpose of this study is to reveal any possible effects or trends on the wall deformation with changes in strata conditions by implementing different combinations of roof, seam, and floor material properties. The model is calibrated by the experiment conducted on a steel-reinforced concrete wall by the NIOSH researchers in the Lake Lynn Experimental Mine. The results show that strong adjacent rock and coal units are the least favorable condition for the survival of the wall subjected to a simulated explosion pressure. The results indicate that changes in the roof and seam conditions can have dramatic effects on the deformation characteristics of the wall when compared to the floor conditions. The results of this study might be enlightening for future BIP RA and seal applications.

**Keywords** Built-in place · Refuge alternative · Seal · Mine explosion · Numerical analysis

## 1 Introduction

Underground coal mining brings a high potential for one of the most frightening hazards, mine explosions. Multiple coal miners can be lost in a single gas explosion accident. In the USA, the Sago Mine Explosion (WV), the Aracoma Alma Mine Fire (WV), and the Darby No. 1 Mine Explosion (KY) were three separate catastrophes in 2006 that resulted in a total of 47 fatalities [1]. This milestone led to improved requirements put into force by Mine Safety and Health Administration (MSHA) and triggered the construction of the Miner Act of 2006 [2–4]. These requirements are mainly related to the underground constructions to isolate an area from active workings; these are seals and build-in-place (BIP) refuge alternatives (RAs). Seals are employed to separate abandoned mining regions from active workings. Their main purpose, from a safety standpoint, is to prevent methane gas that seeps from coal seams in the abandoned area from intruding into active working areas. They are also designed to withstand blast pressures from a possible accidental detonation of the contained gas, or a coal dust explosion within the sealed area [5]. On the other hand, the primary purpose of an RA, including mobile and BIP, is to provide a safe haven for miners who are unable to escape their working location owing to hazardous fumes or a blocked escape route immediately after an explosion. The RA must survive the initiation of the disaster, whether it is an explosion or a fire, to be effective [6]. It would also be advantageous if it could shield the miners inside the RA

✉ Taghi Sherizadeh
sherizadeh@mst.edu

[1] Department of Mining and Explosives Engineering, Missouri University of Science and Technology, Rolla, MO, USA

from the blast effects of secondary explosions. Despite these benefits, existing BIP RA designs are stationary and thus impractical to shift frequently, which makes them very similar to seals from that point of view as well [6].

MSHA subsequent detailed accident investigations into these incidents (The Sago and Darby No. 1 mine accidents) revealed that in both cases, the failure of the seals to withstand the explosion pressures generated in the sealed-off area due to a methane-air explosion was the primary cause of the disasters. However, miners escaped the first tragedy in all these disasters but were unable to leave or successfully separate themselves from the poisonous gases released into the mine environment as a result of the disaster [6]. This report shows the significance of both seals and RAs during such mine accidents. MSHA further stated that the blast pressures created in these mishaps were far more than the mine seals' intended capacity [7]. Kallu [7] also stated that the failed seals in both mines were made of the same acceptable alternative (other than solid concrete block seals) seal material for a 20-psi (0.138 MPa) seal, but none of them were built in the same way as the ones used in the Lake Lynn experimental mine (30 CFR Part 75). MSHA issued "Sealing of Abandoned Areas; Final Rule," which increased the seal design strength and imposed new requirements for the engineering and construction of mine seals by 2008 [8]. In other respects, since the seal practices are similar, the factors that engineers must examine when submitting RA-stopping designs for approval under MSHA's Refuge Alternatives for Underground Coal Mines [Federal Register 2008] and recommendations for coal mine seal design applications [MSHA 2008] were investigated by Office of Mine Safety and Health Research (OMSHR). According to the report, the recommended BIP RA design is very similar to the seal application with reinforced concrete (Trackemas et al. 2015). There are a variety of seals which can be used in underground coal mines in six categories; 1) concrete-like materials with steel reinforcement and reinforcement bar anchorage to rock, 2) pumpable cementitious materials of varying compressive strengths with no steel reinforcement and no hitching, 3) articulated structures such as solid-concrete-block seals and ventilation stoppings made of solid and hollow-core concrete blocks, 4) polymer and aggregate materials without hitching, 5) wood-crib-block seals with or without hitching, and 6) articulated structures such as lightweight blocks with or without hitching [4]. OMSHR created thorough guidelines for RA stopping design applications, as well as specifications for RA stopping designs to serve as an example, using the MSHA seal application guidelines as a reference. The exemplary design is a type of rebar-reinforced concrete wall utilizing recognized design concepts for protective structures in the Unified Facilities Criteria (UFC) [6]. This design can be considered in the first category of sealing techniques, consisting of concrete material with the use of internal rebars as steel reinforcement and additional steel bars to anchorage to surrounding strata.

Seals are split into three groups based on their placement in relation to the mining layout: panel seals, district seals, and cross-cut seals. Seal design engineers should examine all aspects that impact seal performance, such as explosive loading potential, roof-to-floor convergence, and air leakage potential, in each application [5, 7]. ANIOSH report [6] suggests that BIP RAs with a borehole to the surface or a protected compressed air line with a connection to the surface might be constructed at the mouth of each segment. The BIP RA would be constructed in a crosscut or blind cutout, with stopping/door mechanisms set back at the ends to better withstand any explosive forces, however, Zipf et al. [5] stated that crosscut seals are prone to strong convergence and have a significant leakage potential due to high convergence damage near mined out areas. As two or three of the BIP RA's walls are made of mine ribs and one or two explosion-resistant stoppings are built to isolate the region from the rest of the mine, extra support in the roof and ribs has been suggested to prevent excessive convergence damage to RA structures [6].

A thorough and experimental approach is required for estimating explosion resistance capability because it is crucial to understand how these underground constructions respond to explosion blast pressures to assess how well they can keep their occupants and the surrounding area safe. In physical experiments, an actual explosion on a full-scale model might be used. It is possible to gauge the seal or BIP RA's level of damage after an explosion as well as their capacity to withstand explosion blast pressures. Observing the deformation process throughout the experiment, though, can be expensive or dangerous. Additionally, each mine has its own distinct strata conditions, as is the case with this study's focus. Therefore, it can be said that a numerical analysis of deformation under explosion would be a reliable and useful tool to overcome some limitations of experimental studies.

In this study, a steel-reinforced concrete wall to be used in seal and BIP RA applications is simulated to examine the performance during an explosion for a coal mine model with different strata conditions using dynamic analysis by a distinct element code [9]. The reason for the use of a distinct element method is to observe the effect of contact behavior between the concrete wall and coal seam, roof, and floor later in this study. The main purpose of this study is to reveal any possible effects on the wall deformation with changes in strata conditions by implementing different combinations of roof, seam, and floor. This study aims to identify quantitative changes in the deformation of the concrete wall during the explosions and to capture any trend with the increasing and decreasing strength of three varying units of a typical coal mine environment. The concrete wall simulated in the

models is the experimental study conducted by Zipf et al. [4] at the NIOSH Lake Lynn Laboratory used for the structural tests. Since the roof, rib, and floor rocks in the experimental mine consist of limestone, the simulations are firstly calibrated using the reported limestone strata conditions. Then, the models are generated in different combinations of typical coal mine environments using this calibrated initial model.

## 2 Modeling Methodology

The numerical model consists of certain steps including geometry developing, selecting proper material properties, assigning material models and contact models, boundary conditions, in-situ stress initialization, zonking for plastic models, excavation and fill commands to simulate the concrete wall, and dynamic loading. These steps are scrutinized under the following sub-headings.

### 2.1 Geometry, Discretization, and Boundary Condition

A mine model with 2.1 m of seam height was first simulated by developing a 3D geometry of 30 × 30 × 2 m dimensions in *x*, *z*, and *y* directions, respectively. Various mesh sizes were chosen based on the area of interest and influences in the discretization, as well as the required boundary conditions. The mesh boundaries and boundary conditions were chosen so that they would have minimal impact on the area of interest. The geometry was zoned with three different edge lengths of tetrahedral elements; these are the excavation, intermediate, and the rest zones from finer to coarser mesh. The objectives of assigning different levels of mesh size and tetrahedral elements are to decrease the required time to solve a single model since the use of static and dynamic time integration solutions for both strata and explosion simulation, respectively, cause high computational costs. To prevent abrupt change among these zones, the edge lengths were selected to be 10, 20, and 50 cm (see Fig. 1). It should be noted that the models that have been run with 10 cm of mesh size showed similar results with the model having gradually increased mesh sizes in preliminary models. Boundary conditions were imposed to be fixed displacement on all sides of the model with roller boundaries.

### 2.2 Constitutive Model

Since the aim of the study is to reveal the effects of different strata conditions on the deformation of underground concrete walls, both elastic and plastic combinations were simulated to also bring out the possible effects of elastic and plastic behaviors of the roof and seam on the wall. Two series of combinations for distinct material properties of roof, seam, and floor were conducted. For the elastic runs, an isotropic elastic constitutive model was assigned to all three units, the simplest model with the fewest input parameters, governed by bulk and shear modulus in this study. The constitutive models employed for the plastic simulations were the elastic-perfectly plastic Mohr–Coulomb on the roof and floor strata and strain-softening on the coal seam. The Mohr–Coulomb model with non-associated shear and associated tension flow rules is the basis for this strain-softening concept. These constitutive models require four key input parameters: cohesion, $c$, friction angle, $\phi$, dilation angle, and tensile strength, $t_0$. The uniaxial compressive strength, $C_0$ of a rock, is determined by cohesion and friction angle as in

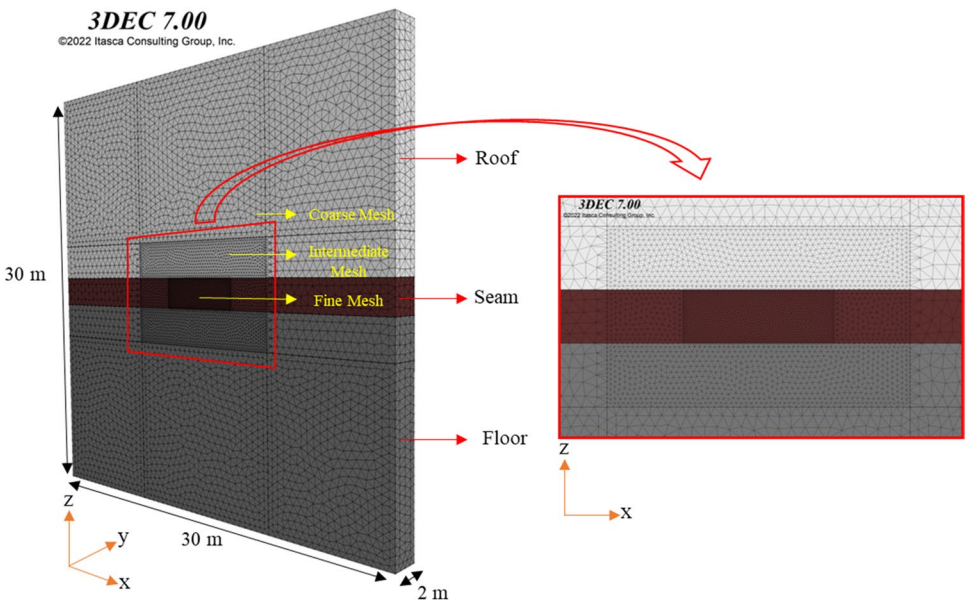


**Fig. 1** Model geometry and mesh discretization

Eq. (1) according to a Mohr–Coulomb strength model. The distinction, however, is that at the commencement of plastic yield, the cohesion, friction, dilation, and tensile strength may soften or harden, whereas those quantities are supposed to be constant in the Mohr–Coulomb model [9]:

$$C_0 = \frac{2c\cos\phi}{1-\sin\phi} \tag{1}$$

As Esterhuizen et al. [10] state, the authors' laboratory testing and published results in Ryder and Jager [11] and Brady and Brown [12] appear to imply that for small-scale samples, the majority of the cohesiveness is lost by over 0.5% plastic strain. The rate of strain loss is predicted to vary depending on the kind of rock and the quantity of clay or carbonaceous elements in the sample. However, there are no sufficient test findings to support utilizing varied softening rates for different materials. Therefore, in this study, as Esterhuizen et al. [10] assumed, after 0.5% strain, all rock materials are modeled with a 90% loss of cohesiveness. After 2% strain, the residual cohesion is predicted to drop linearly to 1 kPa, implying that the rock matrix cohesiveness is completely degraded at large strain.

Table 1 summarizes the elastic and plastic initial values for input parameters of a suggested suite of "numerical rocks" as well as a geologic description. The laboratory-scale values are converted to field-scale or model-scale values from point load experiments conducted during geologic logging. To achieve the field scale and hence the input parameters to the numerical model, the laboratory values for rock and coal are reduced by a factor of 0.56 [13]. Rusnak [14] presents coal seam parameters based on a substantial amount of rock mechanics testing where the cores were subjected to bulk density, uniaxial compressive strength, Young's modulus, and indirect tensile strength tests with a total of 3468 tests completed. Therefore, while the rock parameters are taken from Zipf et al. [13], coal parameters are from Rusnak [14].

## 2.3 Joint Constitutive Model

When utilizing numerical modeling tools like 3DEC, the normal and shear stiffness of contacts are needed inputs for simulating ground control problems. The contacts created between the units (the roof and seam/the seam and floor) were controlled by the elastic joint constitutive model. Published data on the stiffness of rock joints, according to Li et al., [15], shows that normal and shear stiffness vary greatly and that the numerical analysis' outcome is substantially influenced by the huge variance in stiffness. Esterhuizen [16] provides a set of input parameters for the numerical modeling of coal pillars assumed to be satisfactory after experimenting with a variety of inputs and comparing the results to empirical data based on the requirements of matching the Bieniawski strength equation and obtaining identical failure depths and stress gradients as seen in the field. Although the provided input parameters cover interface friction angle, cohesion, and tensile strength with normal and shear stiffness values (100 and 50 GPa/m respectively), since the joint constitutive model is assumed to be elastic, the plastic material properties were not considered.

## 2.4 Initial Stress

Different approaches were used to establish in-situ stresses in the coal seam and rock layers. For coal seam in situ stress initialization, Liu et al. [17] provided Eqs. (2)–(4)]. In Mohamed et al.'s [18]' study, the in situ stresses in the rock layers were calculated using Esterhuizen's [19] (unpublished) recommendations [Eqs. (2), (5), and (6)].

**Table 1** Input parameters for rock and coal units used in the models (taken from Zipf [13]). (* taken from Rusnak [14])

| Description | UCS, $C_0$ (MPa) | Young's modulus, $E$ (GPa) | Cohesion, $c$ (MPa) | Friction angle (°) | Dilation angle (°) | Tensile strength, $t_0$ (MPa) |
|---|---|---|---|---|---|---|
| Claystone, fireclay | 3.6 | 3.0 | 1.2 | 22 | 10 | 0.3 |
| Black shale, gray shale | 10.0 | 5.0 | 3.3 | 24 | 10 | 1.0 |
| Siltstone, gray shale | 19.0 | 7.0 | 6.0 | 26 | 10 | 1.9 |
| Siltstone, sandstone | 35.0 | 10.0 | 10.0 | 30 | 10 | 3.5 |
| Sandstone | 53.0 | 15.0 | 14.0 | 34 | 10 | 5.2 |
| Limestone | 78.0 | 20.0 | 20.0 | 36 | 10 | 7.7 |
| *Bright coal (BC) | 5.0 | 0.83 | 0.83 | 30 | 10 | 0.25 |
| *Banded bright coal (BBC) | 11.0 | 2.55 | 1.90 | 30 | 10 | 0.66 |
| *Dull coal (DC) | 19.0 | 3.52 | 3.22 | 30 | 10 | 1.02 |

The simulated mining conditions are typical US coal mine environments, as Mohamed et al. [20] used an overburden depth range of 91–320 m, and only one certain depth of 320 m was assigned to model the extremum condition in this study:

$$\sigma_v = \gamma \times Z \tag{2}$$

$$\sigma_{Hc} = 1.174 + 0.024 \times Z_c \tag{3}$$

$$\sigma_{hc} = 0.018 \times Z_c - 1.475 \tag{4}$$

$$\sigma_{Hr} = 0.313 + 0.027 \times Z_r + 0.000278 \times E_r \tag{5}$$

$$\sigma_{hr} = 0.65 \times \sigma_{Hr} \tag{6}$$

where $\sigma_v$ is the maximum vertical stress for both the coal seam and the rock layers and is the specific weight of the geologic units in MN/m$^3$, $\sigma_{\mathrm{Hc}}$ and $\sigma_{\mathrm{hc}}$ are the maximum and minimum horizontal stresses, and $Z_c$ and $Z_r$ are the coal seam and rock layers depths in meters, respectively. $E_r$ is Young's modulus of rock layers in MPa, while $\sigma_{\mathrm{Hr}}$ and $\sigma_{\mathrm{hr}}$ are the maximum and minimum horizontal stresses of the rock layers, respectively. All stress units are measured in megapascals (MPa).

### 2.5 Excavation Stages of Elastic and Plastic Model

An opening in the coal seam to represent the crosscut for the analysis scenario was created by excavation with 5.7 m width × 2.1 m height. Before the excavation of the zone where the steel-reinforced concrete wall will be constructed, the model was solved to reach equilibrium under specified in situ stress conditions. Upon the equilibrium, the excavation is carried out with different procedures for elastic and plastic models to prevent excessive computational costs. For the elastic models, the full excavation is applied in one stage without any strength reduction of the coal in that zone. However, the plastic models include two additional stages, zonking and supporting, to capture the more realistic behavior of the zone.

Stresses on elements in the excavation zone can be gradually reduced to avoid transferring stresses to neighboring elements very quickly. Itasca coined the term "zonk" to describe a method of reducing stress gradually and incrementally within the elements to solve the numerical problem accurately. This method can be used to simulate the effect of time and pseudo-time behavior for the changing mining geometry in terms of time in days to years [21]. Using this procedure, the material stiffness in the area to be excavated was softened to 1/100 of the initial values after 100 stages for all plastic models.

### 2.6 Support

The excavation was supported at the ribs and roof for all plastic models with the same supporting combinations independent of the coal seam type. Itasca codes contain multiple structural support features [9]; most rock or cable bolts in real coal mining applications are represented by the structural element "cable," which expresses rock support as an axial force along a line [13]. The structural features of the steel, such as elastic modulus, cross-sectional area, and yield strength, as well as the structural characteristics of the anchor, are all properties that the "cable" element requires. Most anchors used with rock and cable bolts in US mines currently consist primarily of resin with a little amount of cement grout [22]. In 3DEC, the anchor parameters are represented by two properties: the grout stiffness and the grout's cohesive strength. Apart from the conventional steel properties, the grout stiffness values are 1 MN/m and 1 MN/m/m grout cohesion and stiffness, respectively. The installation of three bolts was simulated at the ribs with 1.2 m and 90 cm of length and spacing, respectively. The roof was supported by 5 bolts with 2 and 2.6 m of lengths with 95 cm of spacing; 2.6 m of the bolt was installed in the middle of the roof, as can be seen in Fig. 2. The lengths of the bolts were inspired by Esterhuzien et al.'s study [10].

### 2.7 Concrete Wall

The zonked and supported excavation is partially filled with the steel-reinforced concrete using the "block fill command" of 3DEC. The block excavate command keeps all the geometry from the first excavated block in memory. The block fill command replaces the original block with a new one. Because the block excavate command joins blocks, if only a piece of the excavation is to be filled, a specific process must be used [9]. This process includes in order of filling the excavation, unjoining the blocks in the fill volume, cycling the model zero to create sub-contact between filled blocks and excavated ones, re-excavation of blocks that are not filled at this step, and verification of the properties of zones and joints.

Under a multi-axial condition of stress, concrete is a heterogeneous, cohesion-frictional material that exhibits complex nonlinear behavior. Understanding the mode of failure of concrete structures requires a thorough understanding of the entire stress–strain dynamics. The filled zone with the geometry of 2.1 m in height, 5.7 m in width, and 0.30 m in thickness (see Fig. 3), which corresponds to the concrete wall, was simulated using a strain-softening constitutive model. The parameters used in the model were density, bulk and shear modulus, cohesion, friction angle, and tensile strength. The ultimate values for the concrete wall will be given in the following sections upon the calibration.

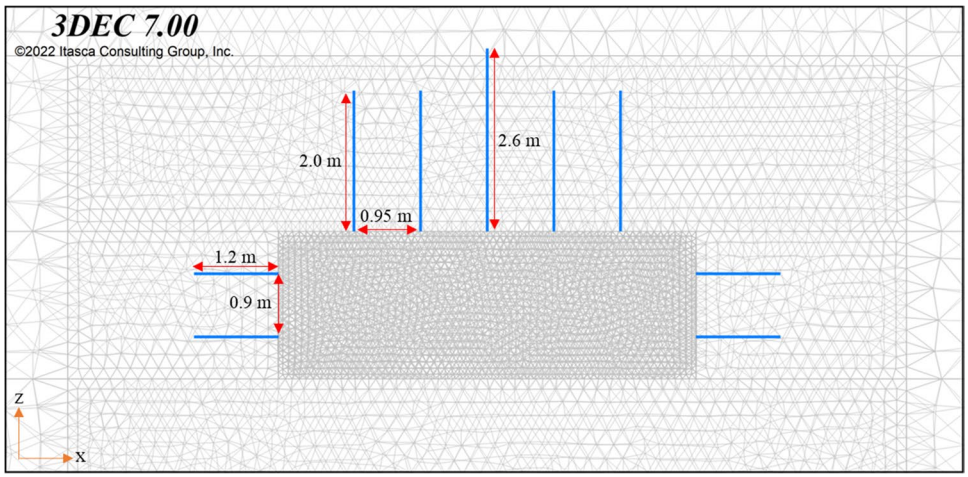


**Fig. 2** Support configuration of the plastic models

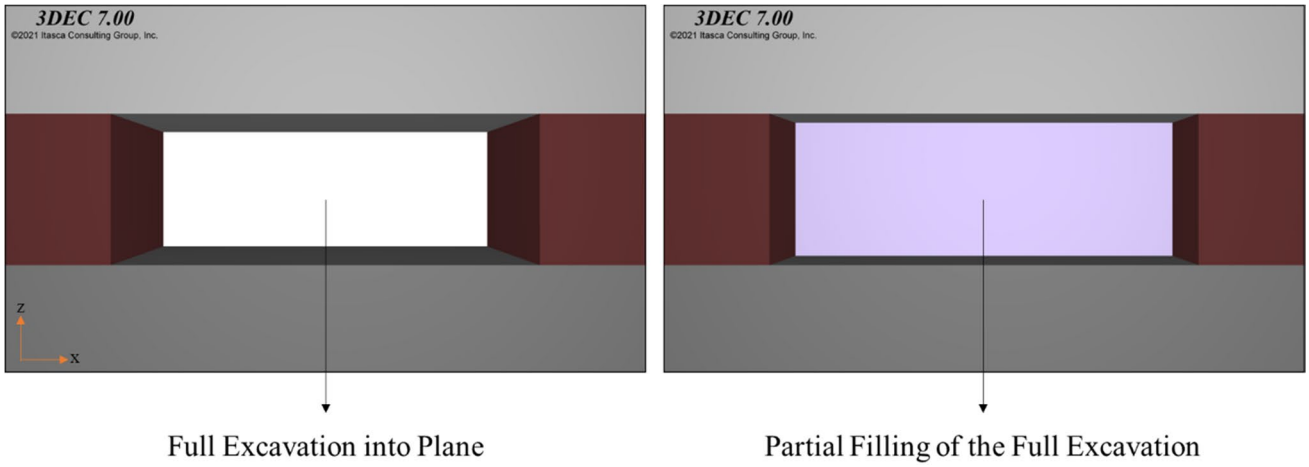


**Fig. 3** The views of the models after the excavation and partial filling to simulate the concrete wall

Softened parameters were the cohesion and tensile strength while keeping the friction angle constant. After 0.3% strain, the concrete wall was modeled with a 50% loss of cohesiveness, 70% loss at 0.35% strain, and 90% loss at 0.40% strain. For the tensile strength, it was assigned to be 95% loss at 0.3% strain, 98% loss at 0.35% strain, and 99% loss at 0.40% strain. These softening parameters were taken from Kallu's seal design study [7].

As in the further motivation of this study, the contact behavior between the wall and coal seam and rock units will be studied to reveal its effects on the concrete wall deformation. Therefore, 3DEC was utilized to benefit from the advantages of distinct element modeling. For the scope of this study, the contact of the concrete wall was modeled by the same approach that Kallu [7] implemented. Kallu [7] assigned an elastic perfectly plastic model for the interface in his finite element analysis. The parameters used for the contact are cohesion and internal friction angle with the Coulomb friction model, the cohesion-less contact with 58° of friction angle. In addition to the constitutive model and contact model of the concrete, the steel reinforcement will be given in the following calibration section.

## 2.8 Dynamic Loading

There are a variety of techniques to solve the dynamic equations of equilibrium in structural dynamics that can be employed successfully. Numerical analysis is the most reliable interpolation and extrapolation approach among the others because of its usefulness in solving complex problems. The most commonly used approaches in numerical assessments are static and dynamic analyses, which are based on the equilibrium principle and energy conservation, respectively. The main difference is the duration of the applied stresses. Because explosive loading lasts only a few milliseconds, the blast pressure acting on the structure is referred to as an impulse. In the analysis of mechanical components subjected to impulsive stimulation, the effect of

stress wave propagation within the material is critical. The stress wave will cause the stress redistribution in mechanical components to change over time, causing stress levels to rise above those expected by static loadings. The D'Alembert principle can be used to derive equations that regulate the dynamic response of a blast-resistant structure subjected to explosive loading, which can then be written into the element formulation as in Eq. (7) [23]:

$$[M]\{\ddot{d}\} + [C]\{\dot{d}\} + [K]\{d\} = \{F^{ext}\} \tag{7}$$

where $[M]$, $[C]$, and $[K]$ are the mass matrix, damping matrix, and stiffness matrix of the whole structure, respectively.$\{d\}$, $\{\dot{d}\}$, $\{\ddot{d}\}$ are the system nodal displacement, velocity, and acceleration, respectively.

The direct integration is implemented in the solution algorithm, and Eq. (7) can be used to obtain the time history of the displacement and stress fields. The presence of damping is an important parameter in dynamic analysis because the damping in the numerical simulation should match the energy losses in the natural system when subjected to a dynamic loading in magnitude and form. Rayleigh damping is widely employed in time-domain applications to give damping that is approximately frequency independent over a limited range of frequencies [9]. In 3DEC, there are two forms of damping: mass proportional and stiffness proportional. Mass-proportional damping exerts a force in the opposite direction of the velocity that is proportional to absolute velocity and mass. Stiffness-proportional damping delivers a force to contacts or stresses in zones that is proportional to the incremental stiffness matrix multiplied by relative velocities or strain rates. Both types of damping can be used alone or in combination in 3DEC. Rayleigh damping is the use of two types of damping in tandem [24]. Proportional Rayleigh damping is commonly employed in the continuous analysis of structures to damp the natural oscillation modes of the system. In dynamic finite-element analysis, a damping matrix, $C$, is formed with components proportional to the mass ($M$) and stiffness ($K$) matrices, Eq. (8),

$$C = \alpha M + \beta K \tag{8}$$

where $\alpha$ = the mass-proportional damping constant and $\beta$ = the stiffness-proportional damping constant.

To define these two parameters, 3DEC allows the use of two inputs to be the critical damping ratio and fundamental frequency. For multiple degrees-of-freedom systems, the critical damping ratio, or the fraction of critical damping, at any angular frequency of the system can be found in Eq. (9) [23]:

$$\alpha + \beta\omega_i^2 = 2\omega_i\xi_i \tag{9}$$

From the variation of the normalized critical damping ratio with the angular frequency curve, the minimum frequency can be defined where the mass and stiffness-proportional damping curves intersect with Eq. (10).

$$f_{\min} = \omega_{\min}/2\pi \tag{10}$$

According to Biggs [25], the damping of materials varies between 2 and 10%, 2–5% for geological materials, and 2–10% for structural systems. In this study, the damping ratio is taken to be the values found from an experimental study on concrete material, to that study, the experimental results show that with a signal center frequency of 20–100 kHz, the damping ratio is 0.01–0.06, satisfying the assumption of a small damping ratio [26]. Therefore, the damping parameters were assumed as 5% of the damping ratio with 50 kHz center frequency in this study. The applied dynamic loading parameters will be given in the following section.

## 3 Calibration of the Reinforced Concrete Wall

Prior to 2006, when the former 20-psi explosive pressure design requirement was applied to mine seals, 44 different seal structures were tested, and Zipf et al. [4] presented this series of tests, varying the applied loading or pressure–time curves ($P$–$t$) with the measured displacement–time ($D$-$t$) curves. NIOSH performed a testing program for seals designed to fulfill the previous 20-psi pressure design criteria for seals from 1997 to 2008. The program included testing six different categories of seal constructions, which were classified by the principal seal building material and procedure. The first category of these constructions is made of concrete or concrete-like materials such as shotcrete or gunite with internal steel reinforcement and additional steel reinforcement bars that anchor to the surrounding rock as in the scope of this study. Only two tests on seals made of concrete-like materials with internal steel reinforcement that met the reinforced concrete seal criteria were carried out.

### 3.1 Experimented Concrete Wall

As mentioned, the seal is made of concrete, steel reinforcement bar, and reinforcement wire. The seal is anchored to the surrounding rock by steel reinforcement bars. It has also a three-dimensional welded wire space frame termed an Insteel 3-D panel. The back is an Insteel 3-D panel with the stayform backing, and the front panel is without backing, #3 steel reinforcement bars laid horizontally from rib to rib within the panels, a plane of vertical #8 reinforcement bars and #8 reinforcement bar anchors into the roof and floor in front of each panel, and horizontal #8 reinforcement bar anchors into each rib make up the structural components of

the seal with the use of grade 60 steel for both rebars and anchors (see Figs. 4 and 5 for the detailed drawings).

A shotcrete machine is used to completely fill the panels with a fast-setting concrete mix applied from the front side of the seal measuring 30 cm in thickness. Vertical holes are drilled to a depth of at least 30 cm in two sets into the roof and floor and uniformly placed across the entry on fewer than 60 cm centers. The front and back rows' vertical holes are offset from one another. Three horizontal holes, each 30 cm deep and 60 cm apart, are bored into each rib, and 0.9 m long #8 steel rebar anchors are grouted into these vertical and horizontal holes [4, 7]. Figure 6 shows the field configuration of the rebars and anchors implemented.

The constructed concrete wall has 2.1 m of height and 5.8 m of width with 30 cm of thickness. As mentioned before, the factors that engineers must consider when submitting RA-stopping designs for approval under MSHA's Refuge Alternatives for Underground Coal Mines and recommendations for coal mine seal design applications were investigated by OMSHR because the seal practices are similar. Therefore, the recommended BIP RA designs are very similar to the seal application with reinforced concrete like the structure provided by Trackemass et al. [6] (see Fig. 7).

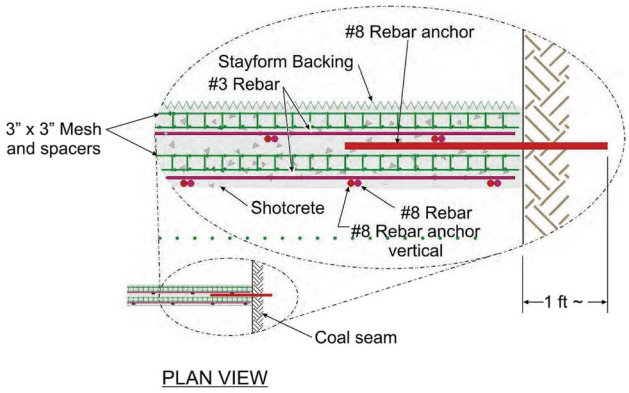


**Fig. 5** Plan view drawing of the structure in detail [4]

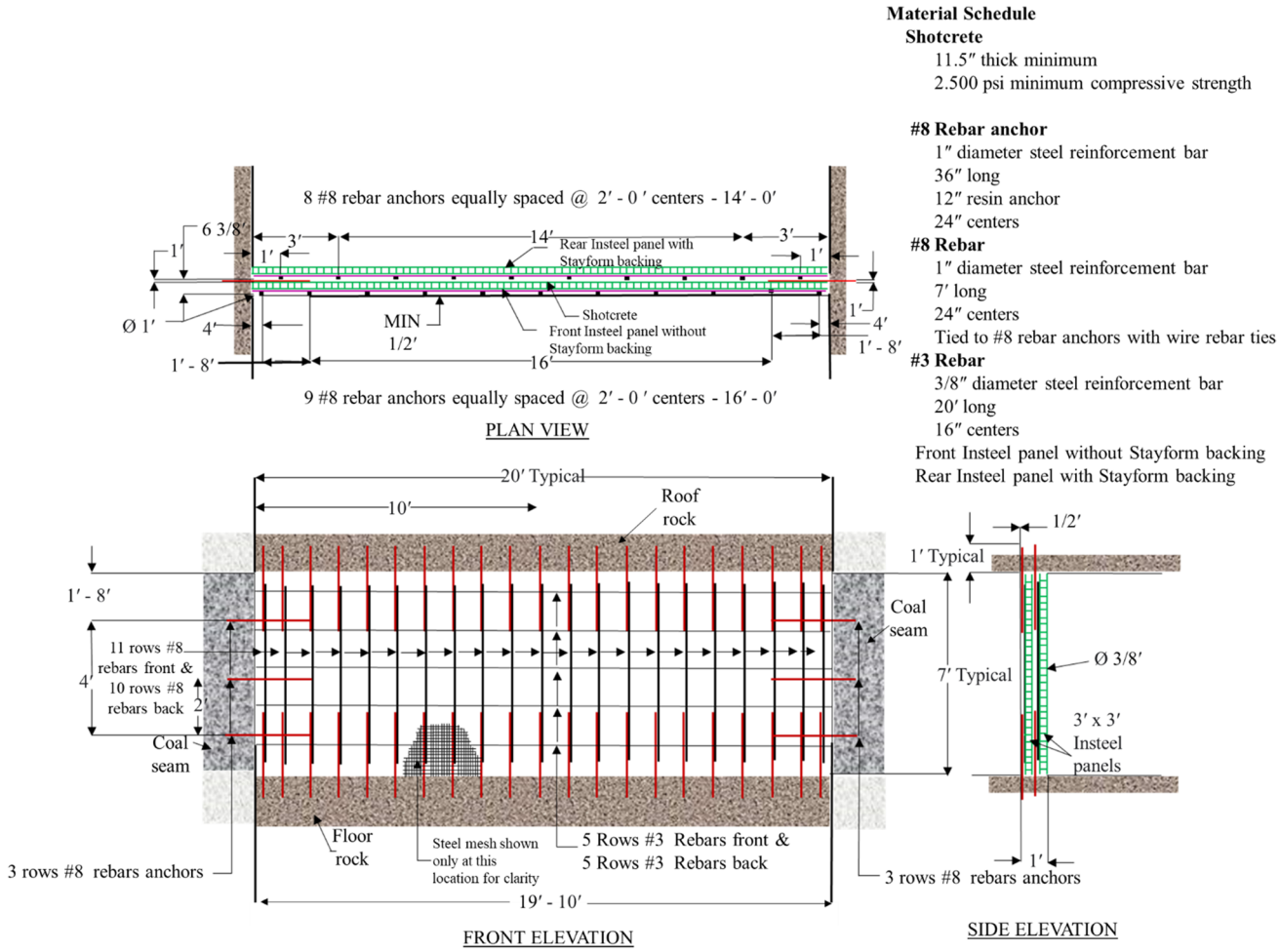


**Fig. 4** The structure configuration used in the calibration; category 1A structure front-, plan-, and side-view drawings [4]

**Fig. 6** The rear Insteel panel with Stayform backing, one plane of vertical #8 steel reinforcement bars and anchors, the horizontal #8 steel reinforcement bar anchors, and the horizontal #3 steel reinforcement bars are seen in this Insteel 3D seal under construction [4]

Pressure transducers were used to monitor the explosion overpressure, and LVDTs were used to monitor the lateral displacements on the outby side of the seal and in the center. The sensor readings show that in 0.1 s the explosion pressure reached a maximum of 0.39 MPa, with lateral displacements of about 2.0 mm. Figures 8 and 9 present the recorded explosion overpressure and the lateral displacements at the center from the explosion test versus time, respectively. The calibration of the models was conducted by the displacement change in the wall with the corresponding applied pressure.

### 3.2 Simulated Model of the Experiment

NIOSH conducted these structural tests on coal mine seals and stoppings at the Lake Lynn Experimental Mine (LLEM) which is comprised entirely of limestone. As this study aims to demonstrate, the strata conditions are crucial parameters in determining the structural performance of BIP RAs; thus, the calibration of the concrete structure experiments conducted by NIOSH accounts for the rock properties found at the LLEM. The authors noticed that the deformation of the concrete wall with the same dynamic loading condition shows different results. Therefore, in the initial models, the boundary conditions of the LLEM were used to calibrate the 3DEC models. According to laboratory studies conducted by Dolinar [27], the roof, rib, and floor rocks in the LLEM are limestone with an intact compressive strength of around 167 MPa and an intact modulus of elasticity of about 66 GPa. According to Esterhuizen [28], the rock mass in the LLEM using the rock mass rating ($RMR_{89}$) standard is of acceptable quality, with an $RMR_{89}$ ranging from 77 to 79. Rock mass stiffness was downscaled that Young's modulus was assumed to be 37 GPa with a Poisson's ratio of 0.25. As a result, the roof, rib, and floor conditions for seal structures built and tested in the LLEM are "rigid" or "unyielding," as

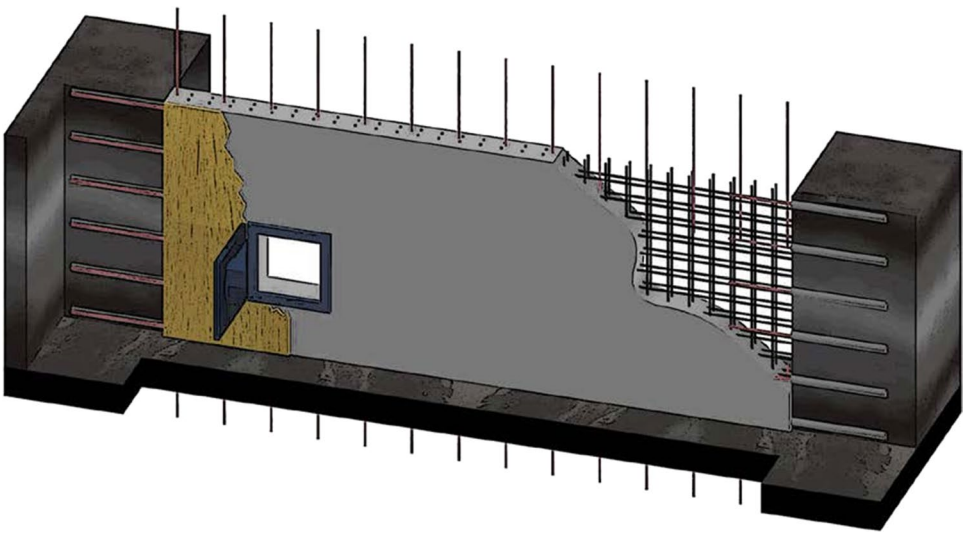

**Fig. 7** Design example for a 15-psi RA stopping using conventional rebar-reinforced concrete [6]

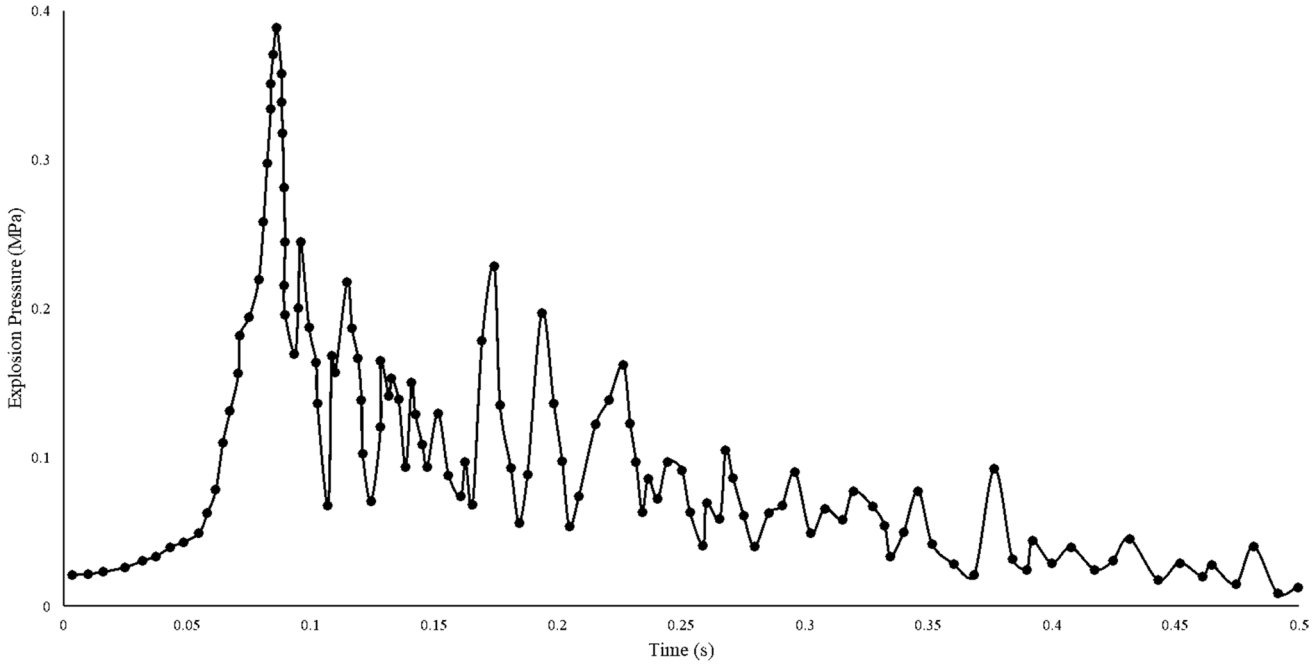


**Fig. 8** Recorded explosion pressure versus time [4]

they represent best-case scenarios. The foundation conditions for the seal tests in the LLEM as described here are not typical of underground coal mines where the roof and floor rock as well as the coal ribs would be less stiff and strong [4]. The in situ stress conditions were assigned using the same equations belonging to the rock conditions [Eqs. (2), (5), and (6)] for the limestone units in LLEM.

As Kallu [7] states that the complete constitutive behavior of the concrete used in the construction of these seals was not available due to the lack of original records on these explosion tests, thus the material parameters were assigned to obtain the best fitting calibration results. Table 2 shows the elastic and plastic material properties assigned to the concrete structures. Several studies suggest that concrete structures with steel wire mesh reinforcement create a localized membrane effect and have better blast-resistant capabilities than a slab without steel wire mesh reinforcement [29, 30]. Since the wire meshes were not simulated for the simplicity of the models, the elastic modulus ($E$) was increased to 40 GPa with the constant Poisson's ratio of 0.2 for the concrete. By changing the input parameters of the concrete wall, while the models were calibrated with the parameters, it has been observed that the most significant input was the tensile strength of the material rather than the

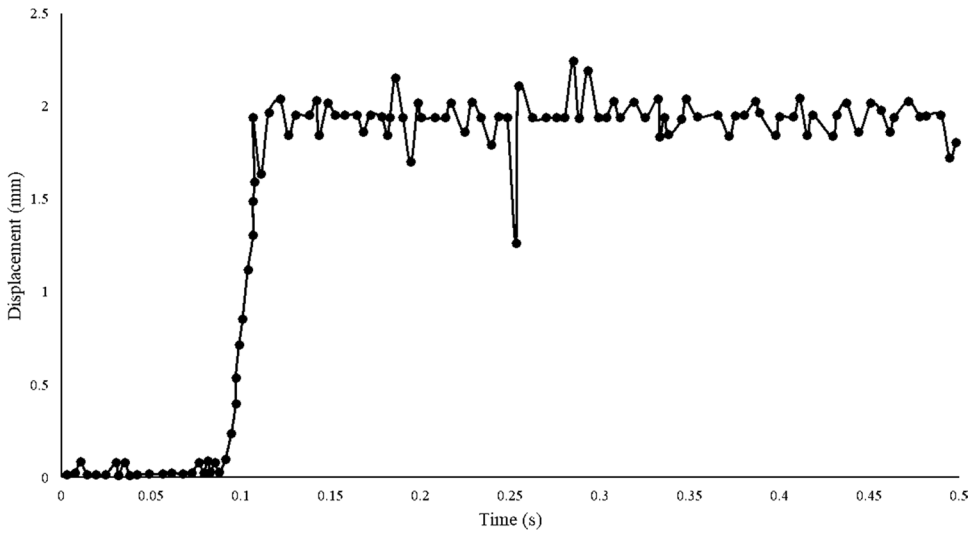


**Fig. 9** Recorded lateral displacement at the wall versus time [4]

**Table 2** Calibrated input parameters for concrete wall

| Parameter | Value |
|---|---|
| Density (kg/m$^3$) | 2200 kg/m$^3$ |
| Young's modulus (GPa) | 40 |
| Poisson`s ratio | 0.2 |
| Cohesion (MPa) | 7 |
| Friction angle (°) | 20 |
| Tensile strength (MPa) | 3.5 |

other plastic material properties. The field application of the reinforcement steels is simulated in the 3DEC model using cable elements as mentioned in one of the previous sections. The 3DEC structural element configuration is presented in Fig. 10. The image on left demonstrates the steel bars to be filled with concrete, and the one on right exhibits the structural elements bored into the ribs, roof, and floor with the transparent mine model meshed geometries in Fig. 10.

By the assigned parameters and applied explosion pressure, the obtained displacement at the center of the wall shows a good agreement with the recorded displacement in the experiment based on the measured rising time. Because the LVDT utilized in the experiment was attached to the structure, the observed displacements are practically constant at roughly 2 mm. While the magnitude of peak displacement predicted by the model does not differ from the actual amount, the residual displacement from the model has an offset of 0.5 mm. Figure 11 shows both the measured and predicted displacement versus the time curve to exhibit the calibration of the models.

The seal withstood the explosion with only minor damage according to field assessments during the explosion test. The 3DEC model anticipates similar outcomes. Figure 12 depicts the displacement contours in the wall for both concrete and steel constructions at 0.125 s. As it can be seen, the steel elements have a similar displacement response as the whole concrete structure and the maximum

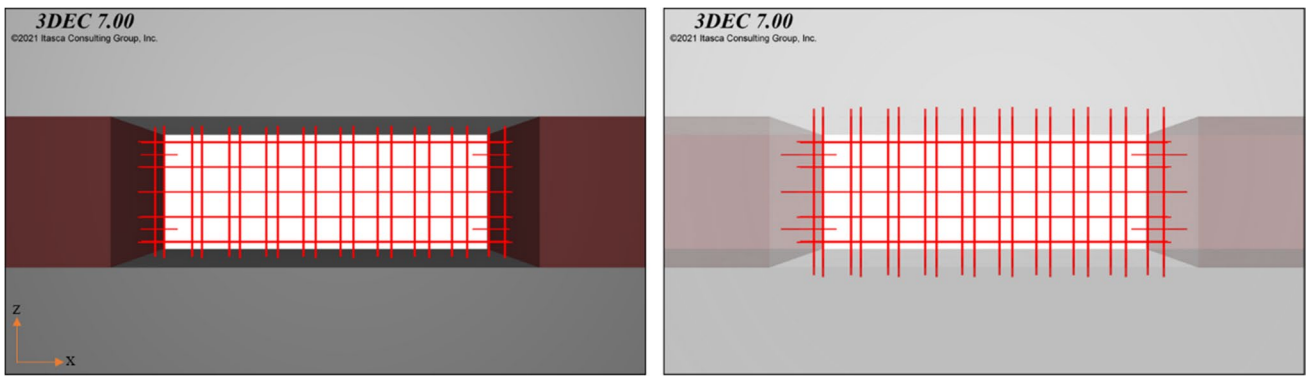


**Fig. 10** The representation of rebars and anchors installed at the simulation (the ones within the concrete at left and the whole structure including the bored anchors on the right)

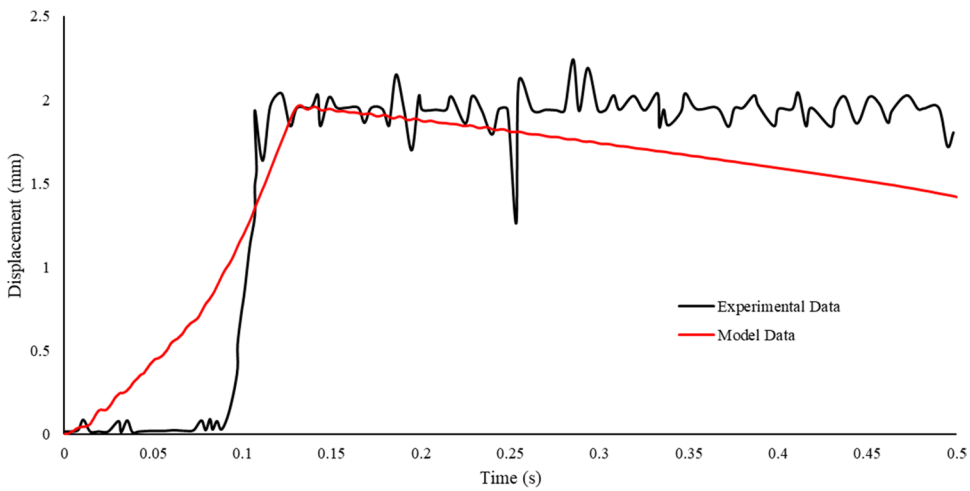


**Fig. 11** The calibration results with the model and experimental displacement versus time

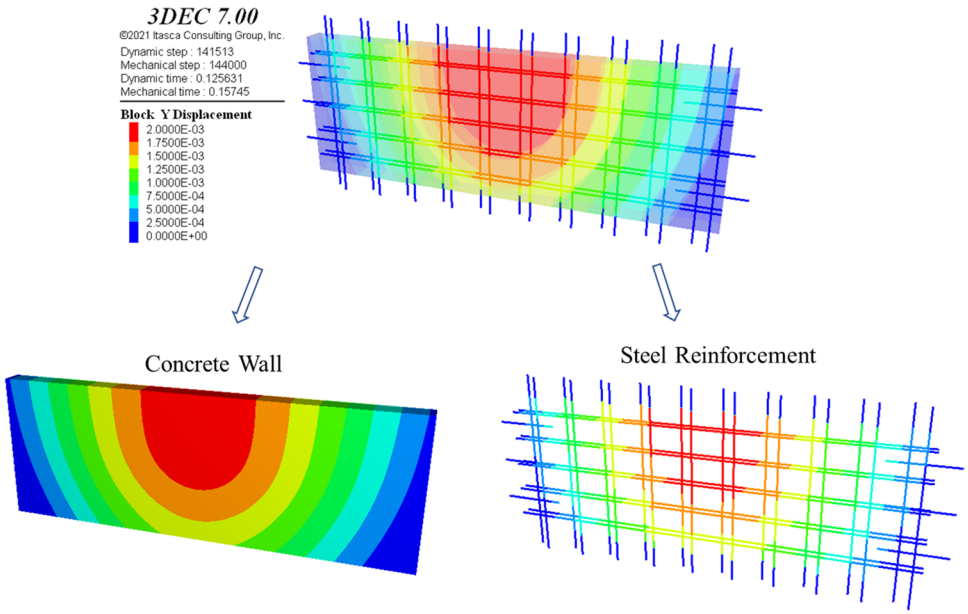


**Fig. 12** Displacement contours for both concrete and steel structures

deformation as expected is observed at the middle of the wall with a slight difference at the roof and floor sides, which will be discussed in the following sections.

## 4 Model Results

A major goal of this research is to uncover any potential effects or changes in strata conditions with various roof, seam, and floor combinations. It was intended to record any trends in the increasing and decreasing strength of these three variable components in a typical coal mine environment, as well as to quantify variations in the deformation of the concrete wall during explosions. The elastic and plastic initial values for input parameters of a suggested suite of "numerical rocks," as well as a geologic description of the rock, are summarized in Table 1. The values shown are reduced laboratory-scale values determined from point load experiments during geologic logging to field-scale or model-scale values [13]. The laboratory or intact values for rock and coal are lowered by a factor of 0.56 to obtain the field or rock mass scale and therefore the input parameters to the numerical model [13]. In this study, the different units were selected for each roof, seam, and floor type. To this determination, roofs were modeled with claystone/fireclay, black shale/gray shale, and siltstone/gray shale units with the increased stiffness and strength of rock properties. Seam and floor were also modeled in a similar fashion to simulate the changing strength parameters; thus, siltstone/sandstone, sandstone, and limestone were used as input of floor unit, whereas BC, BBC, and DC were the input of coal seam modeling. There are two sets of runs to be fully elastic and partially plastic models. In plastic models, only the seam was simulated using strain-softening plastic behavior while the rest was kept elastic. These models were assigned with a code name as "E" and "P" for elastic and plastic models, respectively, following the model number (see Table 3).

These models were analyzed and compared in terms of the lateral deformation on the wall to capture any possible effect or trends with the stiffness and strength of these three units for a typical coal mine environment. To present interpretable results and deduce these possible effects, the peak and residual displacements were exported to a 3D plot for each combination with the unit stiffness values. In other words, independent of the plastic and elastic models, the layers (roof, seam, and floor) were represented with Young's modulus values in the plot axes. The surfaces were created using the data points with one of the simplest interpolation approaches, inverse distance weighting with the power of 2. A neighborhood around the interpolated point is defined, and the observation values within this neighborhood are weight averaged where the weights decrease as the distance increases. Note that the 3D plots are revolved around their axes for their most favorable position to make them easier to understand the trends.

### 4.1 Effect of Overlying Strata

The effects of roof conditions were compared using peak and residual displacements of E/P-1–9, 10–18, and 19–27th models with the corresponding seam and floor stiffness values in terms of mm and GPa, respectively. These results are presented in 9 different plots for 3 distinctive roof units of siltstone/grayshale, black shale/gray shale, and claystone/fireclay (see Fig. 13). From the elastic model results, both peak and residual displacements are in the same trend.

**Table 3** Elastic and plastic strata combinations used in the models with corresponding peak and residual displacements on the concrete wall

| Elastic models | Plastic models | Roof | Seam | Floor | E-peak displacement (mm) | E-residual displacement (mm) | P-peak displacement (mm) | P-residual displacement (mm) |
|---|---|---|---|---|---|---|---|---|
| E1 | P1 | Claystone, fireclay | BC | Siltstone, sandstone | 3.840 | 2.890 | 2.010 | 0.269 |
| E2 | P2 | Claystone, fireclay | BBC | Siltstone, sandstone | 1.370 | 0.651 | 0.633 | 0.195 |
| E3 | P3 | Claystone, fireclay | DC | Siltstone, sandstone | 1.310 | 0.621 | 0.626 | 0.189 |
| E4 | P4 | Claystone, fireclay | BC | Sandstone | 4.080 | 3.20 | 1.920 | 0.296 |
| E5 | P5 | Claystone, fireclay | BBC | Sandstone | 1.390 | 0.662 | 0.641 | 0.214 |
| E6 | P6 | Claystone, fireclay | DC | Sandstone | 1.360 | 0.652 | 0.508 | 0.444 |
| E7 | P7 | Claystone, fireclay | BC | Limestone | 4.450 | 3.53 | 1.790 | 0.295 |
| E8 | P8 | Claystone, fireclay | BBC | Limestone | 1.410 | 0.672 | 0.665 | 0.332 |
| E9 | P9 | Claystone, fireclay | DC | Limestone | 1.360 | 0.634 | 0.437 | 0.562 |
| E10 | P10 | Black shale, gray shale | BC | Siltstone, sandstone | 1.320 | 1.090 | 1.910 | 0.021 |
| E11 | P11 | Black shale, gray shale | BBC | Siltstone, sandstone | 3.620 | 2.930 | 0.736 | 0.268 |
| E12 | P12 | Black shale, gray shale | DC | Siltstone, sandstone | 3.650 | 2.940 | 0.648 | 0.250 |
| E13 | P13 | Black shale, gray shale | BC | Sandstone | 1.360 | 0.668 | 2.030 | 0.021 |
| E14 | P14 | Black shale, gray shale | BBC | Sandstone | 3.380 | 2.630 | 0.688 | 0.279 |
| E15 | P15 | Black shale, gray shale | DC | Sandstone | 3.600 | 2.860 | 0.489 | 0.272 |
| E16 | P16 | Black shale, gray shale | BC | Limestone | 1.270 | 0.603 | 2.290 | 0.027 |
| E17 | P17 | Black shale, gray shale | BBC | Limestone | 3.070 | 2.340 | 0.594 | 0.253 |
| E18 | P18 | Black shale, gray shale | DC | Limestone | 3.540 | 2.800 | 0.350 | 0.324 |
| E19 | P19 | Siltstone, gray-shale | BC | Siltstone, sandstone | 1.250 | 0.602 | 2.500 | 0.153 |
| E20 | P20 | Siltstone, gray-shale | BBC | Siltstone, sandstone | 5.550 | 4.670 | 0.776 | 0.560 |
| E21 | P21 | Siltstone, gray-shale | DC | Siltstone, sandstone | 5.480 | 4.660 | 1.380 | 0.941 |
| E22 | P22 | Siltstone, gray-shale | BC | Sandstone | 1.240 | 0.578 | 2.540 | 0.079 |
| E23 | P23 | Siltstone, gray-shale | BBC | Sandstone | 5.390 | 5.050 | 0.707 | 0.302 |
| E24 | P24 | Siltstone, gray-shale | DC | Sandstone | 5.630 | 4.540 | 1.320 | 0.635 |
| E25 | P25 | Siltstone, gray-shale | BC | Limestone | 1.190 | 0.554 | 2.670 | 0.291 |
| E26 | P26 | Siltstone, gray-shale | BBC | Limestone | 5.160 | 4.360 | 0.651 | 0.243 |
| E27 | P27 | Siltstone, gray-shale | DC | Limestone | 5.750 | 4.650 | 1.250 | 0.582 |

Excluding the claystone/fireclay, by the increase in stiffness values of the roof unit, the deformation on the wall is rising. However, this behavior is showing opposite with the claystone/fireclay model. In these models, the deformation in terms of displacement is advancing by the decreasing stiffness in a coal seam. It should be noted that the stiffness

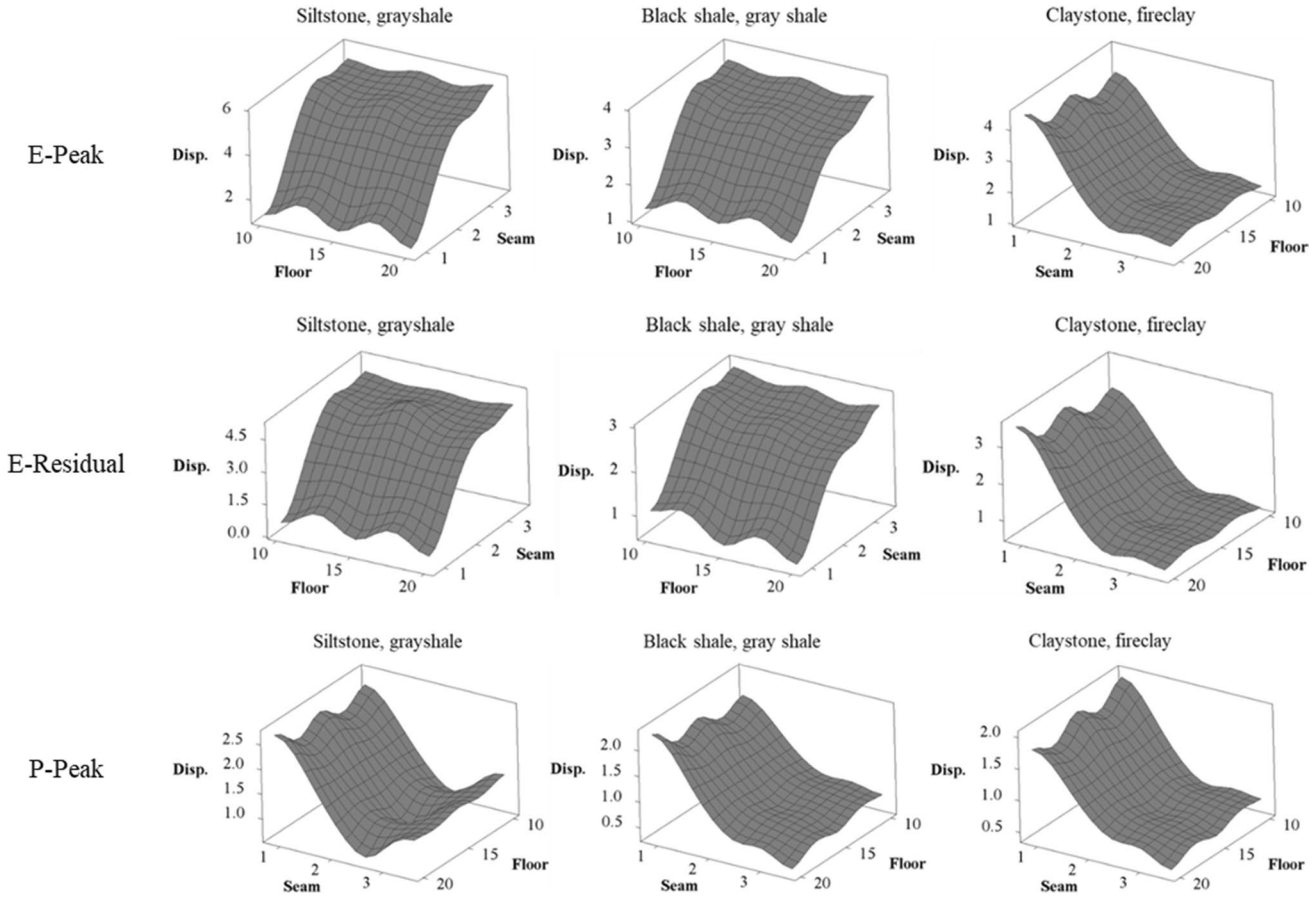


**Fig. 13** Three-dimensional plots of peak and residual deformations (mm) to the corresponding stiffness of seam and floor (GPa) for 3 different roof types

of claystone/fireclay is very close to the strong coal units DC and BBC with a Young's modulus of around 3. On the other hand, in the plastic models, the trend is similar to the elastic models with claystone, fireclay roof, which shows the increasing deformation with decreasing seam stiffness. Nevertheless, it is obvious that the deformation on the wall is escalating by the rise in roof stiffness. The residual deformations are not included in the analyses since the order of magnitude for these are 0.0 mm, and it can be considered that the response of the wall in plastic analyses tends to recover the total strain during and after the explosion.

## 4.2 Effect of Seam

The findings regarding the seam change are also displayed in nine separate charts for three different seam units: BC, BBC, and DC (see Fig. 14). Both the peak and residual displacement trends are in the same direction according to the elastic model results. The distortion on the wall is increasing, excluding the BC, due to an increase in the stiffness values of the seam unit. The BC model, on the other hand, exhibits the reverse trend; in these models, the deformation in terms of displacement is accelerated by the decreasing stiffness in the roof. It should be observed that the stiffness of DC and BBC is quite similar to that of the claystone/fireclay roof unit, which has a stiffness of roughly 3 GPa of E. In the plastic models, on the other hand, it is difficult to claim that there is a rising or decreasing trend in the peak deformation on the wall. In these analyses, the reason why there is no such uniformity in response surface as in the elastic models might be that the support of the ribs is kept constant independent of the seam type; however, it is obvious that the larger deformations on the wall were seen in the elastic models; thus, the elastic models have higher significance to observe any trend for the deformation and stiffness relation.

## 4.3 Effect of Underlying Strata

Figure 15 shows the results of the floor change in nine independent charts for three different seam units: siltstone/sandstone, sandstone, and limestone. According to the

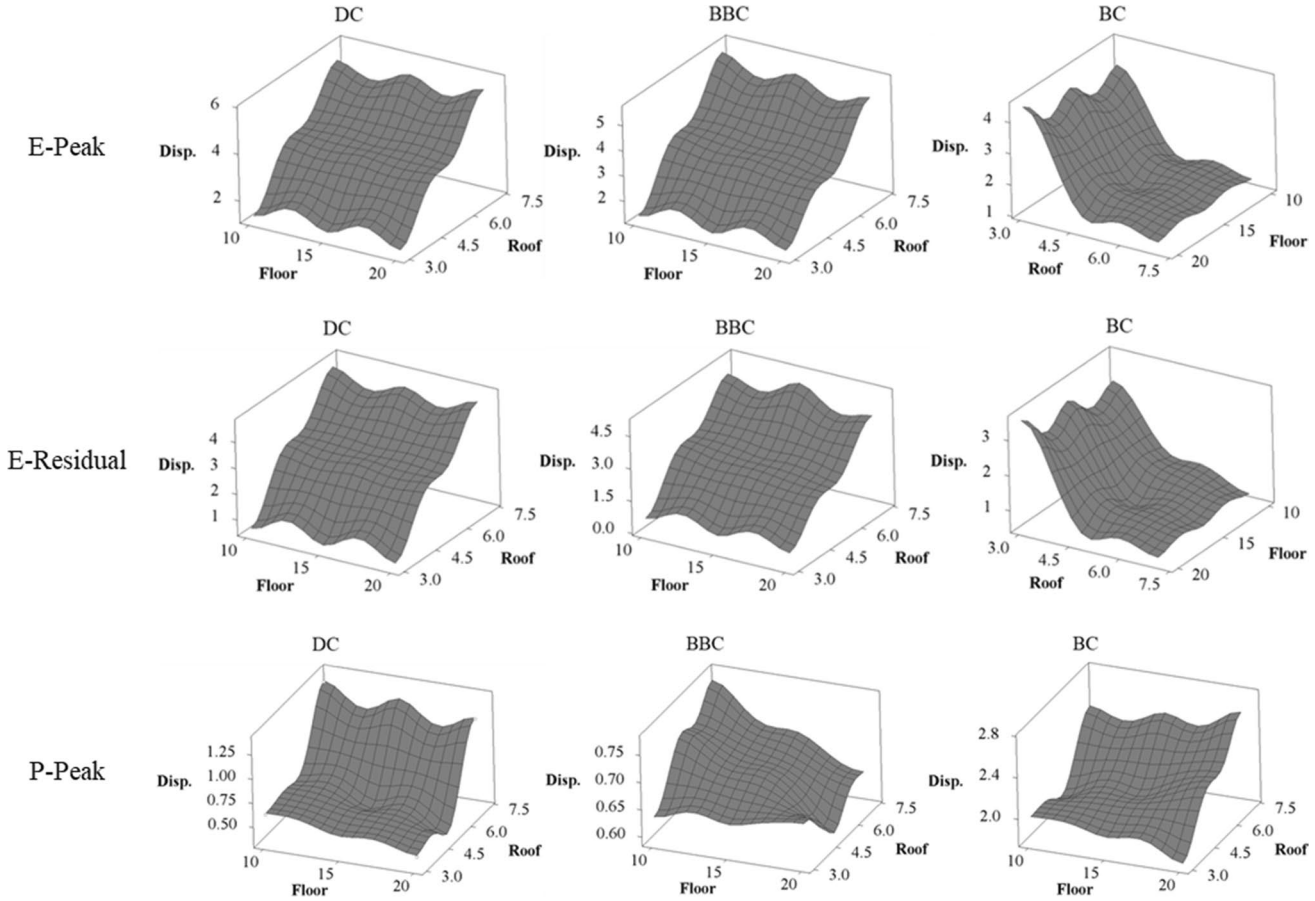


**Fig. 14** Three-dimensional plots of peak and residual deformations (mm) to the corresponding stiffness of roof and floor (GPa) for 3 different seam types

elastic model results, the peak and residual displacement surfaces are quite comparable to one another. The roof and seam axes, on the other hand, show no discernible upward or downward trend. For that stiffness interval of floor, it may be asserted that floor stiffness has no effect on wall deformation. In contrast, while the peak displacement for the plastic models does not vary significantly, the general deformation response of the wall is decreasing in the rising seam stiffness axis. In addition, while looking at the results from the point of view of floor stiffness, the elastic mine models had higher displacement results on the concrete structure than the plastic models.

According to the results of both elastic and plastic models, the concrete wall shows some tensile cracks at the middle zone. Although the values for displacement during and after the explosion simulation are very small, the changes are very significant in terms of yielded elements on the concrete structure. In this manner, Fig. 16 demonstrates the deformation differences over yielded elements between the models with the highest displacement and lowest one. For that purpose, E27 and P27 coded models are taken to be consistent. Whereas the model E27 shows a greater tensile yielded zone, the P27 exhibits a small horizontal tensile crack in the horizontal. It should be noted that the color labels of element states at the rib were assigned to be null to prevent misinterpretation.

Apart from the change in element state on the concrete structure, it is helpful to analyze the stress distribution inside the wall due to both induced stresses transferred from the roof, seam, and floor with the applied stress of the explosion. If the stress distribution is observed, to keep the convenience of the comparisons, the same pair of the models (E27 and P27) was taken into consideration. Figure 17 presents the stress distribution of both E27 and P27 models. For the same combination of the roof, seam, and floor, the elastic and plastic seam model differences create that significant stress distribution change. The concrete

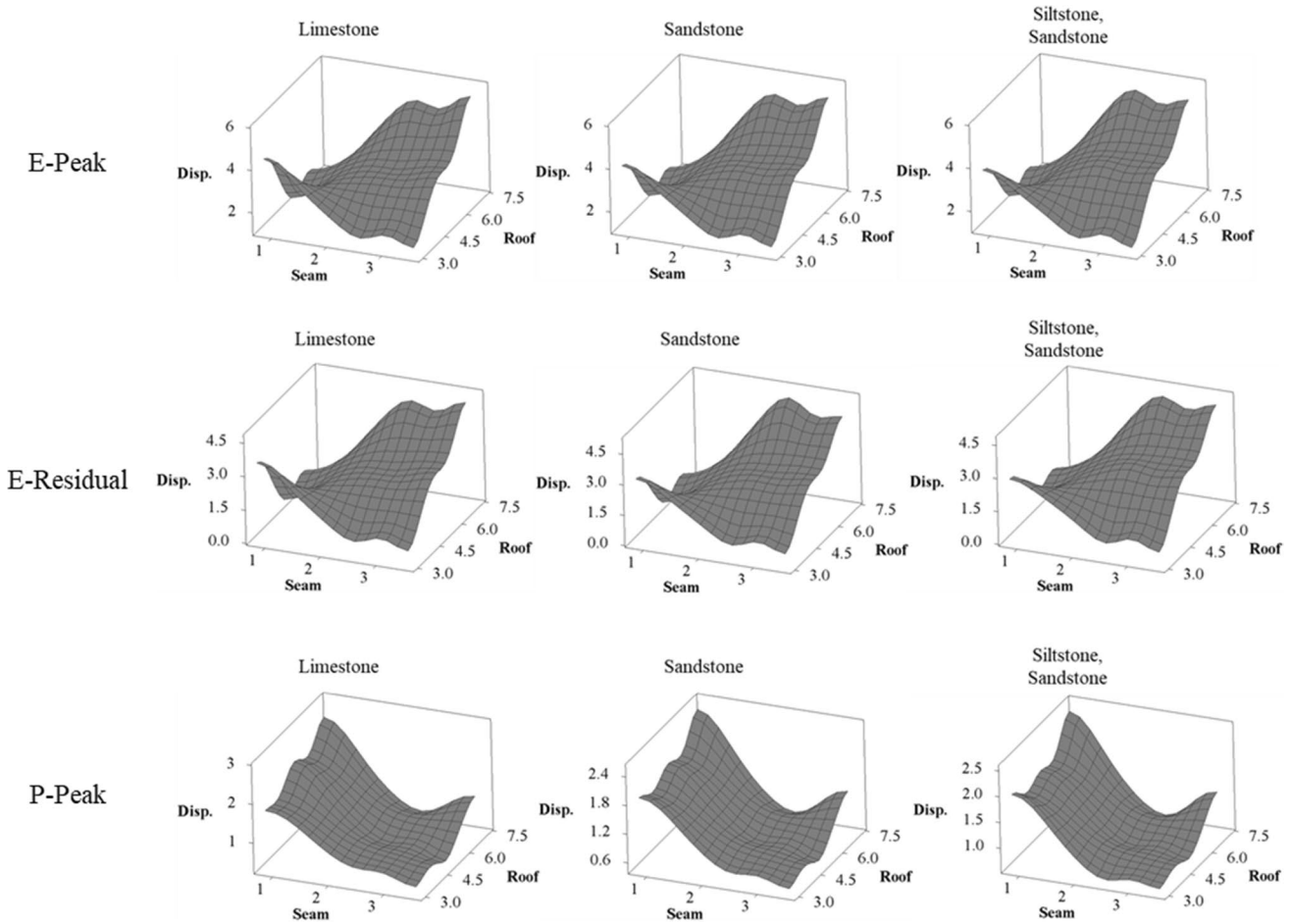


**Fig. 15** Three-dimensional plots of peak and residual deformations (mm) to the corresponding stiffness of roof and floor (GPa) for 3 different seam types

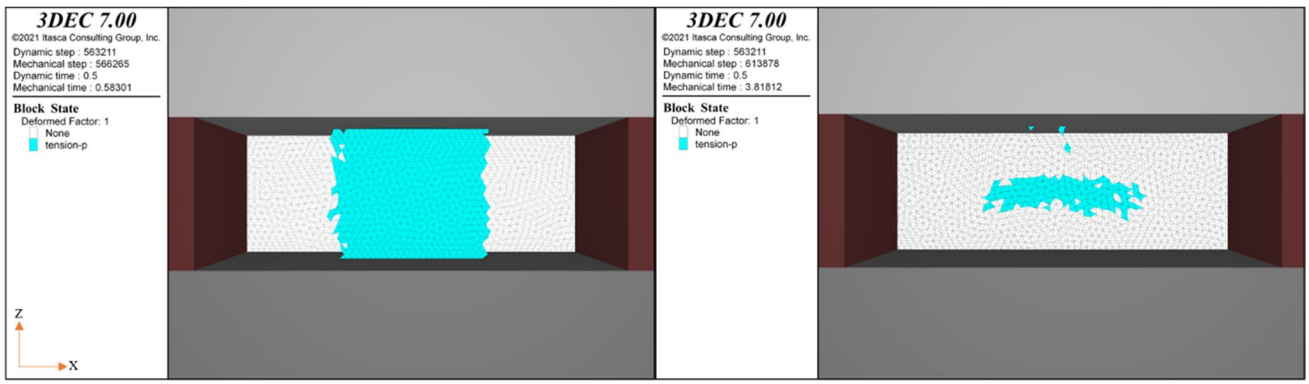


**Fig. 16** Element states on the wall after the explosion for E27 (on left) and P27 (on right)

wall has around 8.3 MPa level of stress in E27, whereas it is about 1.7 MPa within P27, which makes roughly 5 times greater in the fully elastic model than in the elastic–plastic seam modeled run.

## 5 Discussion

Within the results of this study, there are certain outcomes to consider and discuss; these are mainly the concrete

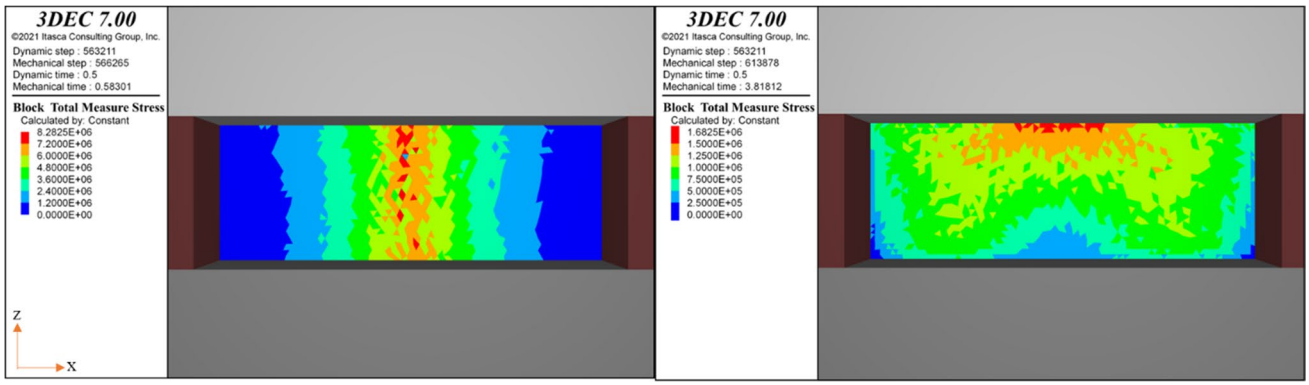


**Fig. 17** Contours of stress magnitude on the wall after the explosion for E27 (on left) and P27 (on right)

structure with its steel reinforcements both inside the concrete and the adjacent rock and coal to bore, the state of these adjacent units especially essential for the stress distribution, contact between the wall and these layers, and contact between the anchored steel components. Since this study does not cover the response of these contact types, these parameters were assumed to be suitable to conduct such a study using the literature data generated.

One of the most significant outcomes of this study is that the deformation behavior of the reinforced concrete wall is slightly different than the one presented by Kallu [7]. The difference is the distribution of the lateral displacement due to the explosion. In that study [7], the displacement contours are quite uniformly distributed in a circular shape from the center to the boundaries in decreasing order of magnitude; however, in this study, the distribution is in a semi-circle shape compassing the roof region with the central part to the boundaries in a declining trend. The reason can be considered that 3DEC can account for the contact behavior between the wall and cross-cut boundaries with its discrete element methodology. In addition, the steel elements are just fixed through that opening perimeter in contrast to the referenced study that fully fixed the structural element for the model simplification. Subsequently, the other reason might be that the fully fixed structural elements do not allow the real gravitational behavior of the concrete structure where the normal load at the floor contact is higher than at the roof due to its own weight.

This behavior of the concrete wall can be thought of as a rectangular plate problem, since it is subjected to a sort of load normal to the surface with boundaries clamped on the edges. In this analysis, two parameters are working as clamps on the wall boundaries; these are the structural elements to anchor through the adjacent layers and stresses distributed from these adjacent layers. Since the steel structure parameters are kept constant in terms of the material properties, the number of elements and the boundary conditions such as fixation at the contact surface between the wall and rock layers, the stress distribution is the governing parameter leading to the change in boundary condition of this plate problem.

Because the stress distributions inside the rock layers are governed by the stiffness, elastic parameters of the units become crucial for the convergence of roof to floor and rib to rib. The 3D surface plots reveal that the convergence of these layers has a positive impact on the survival of the concrete wall by comparing the elastic and plastic models. In the comparison of the general trend and individual matches of elastic and plastic models, the deformation on the wall is significantly decreasing. However, it is also observed that the trend is working in opposite direction considering the models having very close stiffness values of roof and floor. It can be claimed that the transition from deviatoric stresses to hydrostatic stress conditions might be robust to this behavior; thus, the deviatoric stress difference between the roof and coal seam is an advantageous scenario. Because the parameters used for the floor unit are relatively high considering the realistic coal mine environment, there is no significant effect on the deformation of the wall. In the same respect, the deviatoric stresses are so high that they can cause not to see such influence on the concrete wall. In light of the models included in this study, the highest deformation was seen on the model with the stiffest and strongest combinations for each unit, roof, seam, and floor due to the reason stated above.

With the advantage of numerical analysis tools to interpolate or extrapolate the results where the experimental studies are extremely difficult like in this study, the explosion experiment in a real coal mine environment, some model simplifications are needed to prevent the excessive amount of computational cost. Therefore, this study has also some generalizations to be taken into consideration in the related following research. The Mohr–Coulomb constitutive model was used to calibrate and capture the response of the wall, and the more representative model can be created for the sake of the concrete structure. Since the authors do not have any data regarding the real contact behavior of the wall boundaries with the adjacent rock and coal layers, it is

assumed to use a contact model already used in the literature with the taken parameters. In the same approach, the steel structures are also assumed to be the same in contact with the concrete, coal seam, and roof and floor rock units. The study should be conducted to find a more realistic relationship between these structural elements and the rock and concrete units to calibrate the models. Although the results show that the plastic models present lower deformation values on the wall, in other words, the elastic models have a higher significance, the support conditions of the coal seams can be changed with the varying scenario instead of keeping them constant.

## 6 Conclusion

The major goal of this research was to see if there were any effects from different roof, seam, and floor combinations on strata conditions. It was intended to detect any trends in the increasing and decreasing strength of these three variable components of a typical coal mine environment, as well as to quantify variations in the deformation of the concrete wall during explosions. Using 3DEC's "block fill command," the zonked and supported excavation is partially filled with steel-reinforced concrete. The experimental investigation done by Zipf et al., [4] at the NIOSH Lake Lynn Laboratory utilized for the structural testing is the concrete wall simulated in the models. Because the experimental mine's roof, rib, and floor rocks are all limestone, the models are initially calibrated using those limestone strata conditions. The models are then constructed using this calibrated initial model in various combinations of common coal mine conditions.

The different units were chosen for each roof, seam, and floor type in this study. Roofs with increased stiffness and strength of rock properties were modeled with claystone/fireclay, black shale/gray shale, and siltstone/gray shale units to simulate the changing strength parameters; both the seam and the floor were modeled in the same way. For the floor unit, siltstone/sandstone, sandstone, and limestone were used as inputs, while for the coal seam modeling, BC, BBC, and DC were used as inputs. Fully elastic and partially plastic models are available in two sets of runs. Only the seam was simulated in plastic models using strain-softening plastic behavior, while the rest was kept elastic.

The peak and residual displacements were exported to a 3D surface plot for each combination with the unit stiffness values to present articulable results and deduce these possible effects. The wall deformation significantly decreases when comparing the general trend and individual matches of elastic and plastic models. However, the trend appears to be in the opposite direction when considering models with very close roof and floor stiffness values. The transition from deviatoric stresses to hydrostatic stress conditions can be said to be resistant to this behavior, making the deviatoric stress difference between the roof and coal seam an advantageous scenario. There is no significant effect on the wall deformation because the used parameters for the floor unit are relatively high compared to the realistic coal mine environment. Because of the reasons stated above, the model with the stiffest and strongest combinations for each unit, roof, seam, and floor showed the highest deformation of the models included in this study.

There are some simplifications and generalizations in this study that should be considered in subsequent research. The Mohr–Coulomb constitutive model was used to calibrate and capture the wall's response, and a more representative model for concrete structures can be created. Because the authors do not have data on the actual contact behavior of the wall boundaries with the adjacent rock and coal layers, it is assumed that they will use a contact model that has been used before with the parameters they have chosen. Steel structures are assumed to be the same in contact with concrete, coal seams, and roof and floor rock units in the same way. To calibrate the models, a study should be conducted to find a more realistic relationship between these structural elements and the rock and concrete units. Although the results show that the plastic models have lower deformation values on the wall, the elastic models have a higher significance, and the support conditions of the coal seams can be changed rather than kept constant with the varying scenario. In addition, some artificial values for all roof, seam, and floor conditions can be simulated to reveal the effects of stiffness and strength changes in more detailed charts, such as very low rock parameters for the floor.

**Funding** The authors would like to thank the National Institute for Occupational Safety and Health (NIOSH), CDC-NIOSH BAA 75D301-20-R-67922, for financial support.

**Data Availability** The data will be provided upon request.

### Declarations

**Competing Interests** The authors declare no competing interests.

## References

1. Yantek D, Schall J (2017) Lessons learned from refuge alternative research by NIOSH. Coal Age
2. Fasouletos MA (2007) Parametric design of a coal mine refuge chamber. West Virginia University
3. Mitchell MD (2008) Analysis of underground coal mine refuge shelters. West Virginia University
4. Zipf RK, Weiss ES, Harteis SP, Sapko MJ (2009) Compendium of structural testingdata for 20-psi coal mine seals. IC 9515, U.S. Department of Health and Human Services,National Institute for Occupational Safety and Health, p 143

5. Zipf RK, Sapko MJ, Brune JF (2007) Explosion pressure design criteria for new seals in US coal mines. Dept. HHS, NIOSH IC, 9500:76, Pittsburgh
6. Trackemas JD, Thimons ED, Bauer ER, Sapko MJ, Zipf Jr RK, Schall J, Rubinstein E, Finfinger GL, Patts LD, LaBranche N (2015) Facilitating the use of built-in-place refuge alternatives in mines. U.S. Department of Health and Human Services,National Institute for Occupational Safety and Health
7. Kallu RR (2009) Design of reinforced concrete seals for underground coal mines. West Virginia University
8. Zipf RK Jr, Mohamed KM, McMahon GW (2010) Design and analysis of a new method to test mine seals. National Institute for Occupational Safety and Health (NIOSH), Pittsburgh Pennsylvania USA
9. Itasca Consulting Group Inc (2021) 3DEC Ver 7.0. Minneapolis, U.S.
10. Esterhuizen GS, Bajpayee TS, Ellenberger JL, Murphy MM (2013) Practical estimation of rock properties for modeling bedded coal mine strata using the Coal Mine Roof Rating. In 47th US rock mechanics/geomechanics symposium. OnePetro
11. Ryder J, Jager JA (2002) A handbook on rock engineering practice for tabular hard rock mines, safety in Mines Research Advisory Committee (SIMRAC), Johannesburg, South Africa
12. Brady BHG, Brown ET (2004) Rock mechanics for underground mining. Springer, Dordrecht
13. Zipf K (2006) Numerical modeling procedures for practical coal mine design. In Golden Rocks 2006, The 41st US Symposium on Rock Mechanics (USRMS). OnePetro
14. Rusnak J (2017) Coal strength variation by lithotype for high volatile a bituminous coal in the Central Appalachian Basin. In Proceedings of the 36th International Conference on Ground Control in Mining, pp 198–207
15. Li W, Bai J, Cheng J, Peng S, Liu H (2015) Determination of coal–rock interface strength by laboratory direct shear tests under constant normal load. Int J Rock Mech Min Sci 77:60–67
16. Esterhuizen E, Mark C, Murphy MM (2010) Numerical model calibration for simulating coal pillars, gob and overburden response. In Proceedings of the 29th international conference on ground control in mining. West Virginia University. Morgantown, pp 46–57
17. Liu H, Sang S, Xue J, Wang G, Xu H, Ren B, Liu C, Liu S (2016) Characteristics of an in situ stress field and its control on coal fractures and coal permeability in the Gucheng block, southern Qinshui Basin, China. J Nat Gas Sci Eng PB(36):1130–1139. https://doi.org/10.1016/j.jngse.2016.03.024
18. Mohamed KM, Cheng Z, and Rashed G (2019) Coal rib stability based on the strength reduction of the coal mass model. 53rd U.S. Rock Mechanics/Geomechanics Symposium. https://onepetro.org/ARMAUSRMS/proceedings/ARMA19/All-ARMA19/ARMA-2019-2844/125175
19. Esterhuizen GS (2017) Personal communication
20. Mohamed K, Van Dyke M, Rashed G, Sears MM, Kimutis R (2021) Preliminary rib support requirements for solid coal ribs using a coal pillar rib rating (CPRR). Int J Min Sci Technol 31(1):15–22
21. Spottiswoode SM, Milev AM (2002) A methodology and computer program for applying improved, inelastic ERR for the design of mine layouts on planar reefs. SIMRAC GAP722 final report. Safety in Mines Research Advisory Committee, Johannesburg p 85
22. Dolinar DR, Bhatt SK (2000) Trends in roof bolt application. In: Mark C, Dolinar DR, Tuchman RJ, Barczak TM, Signer SP, Wopat PF (eds) Proceedings: new technology for coal mine roof support. U.S. Department of Health and Human Services, Public Health Service, Centers for Disease Control and Prevention, National Institute for Occupational Safety and Health, DHHS (NIOSH) Publication No. 2000–151, IC 9453, Pittsburgh, PA, pp 43–51
23. Hsieh MW, Hung JP, Chen DJ (2008) Investigation on the blast resistance of a stiffened door structure. J Mar Sci Technol 16(2):7
24. Bathe KJ, Wilson EL (1976) Numerical Method in Finite Element Analysis. Prentice-Hall, Englewood Cliffs, New Jersey
25. Biggs JM, Biggs J (1964) Introduction to structural dynamics. McGraw-Hill College
26. Tian Z, Huo L, Gao W, Li H, Song G (2017) Modeling of the attenuation of stress waves in concrete based on the Rayleigh damping model using time-reversal and PZT transducers. Smart Mater Struct 26(10):105030
27. Dolinar DR (2008) Personal communication
28. Esterhuizen GS (2008) Personal communication
29. Li J, Wu C, Hao H, Su Y (2017) Experimental and numerical study on steel wire mesh reinforced concrete slab under contact explosion. Mater Des 116:77–91
30. Wei J, Li J, Wu C (2020) Behaviour of hollow-core and steel wire mesh reinforced ultra-high performance concrete columns under lateral impact loading. Int J Impact Eng 146:103726